

# Uncertainties in the Anti-neutrino Production at Nuclear Reactors

Z. Djuric<sup>1,\*</sup>, J.A. Detwiler<sup>2,†</sup>, A. Piepke<sup>3</sup>, V.R. Foster Jr.<sup>4</sup>, L. Miller<sup>5,‡</sup> and G. Gratta<sup>5</sup>

<sup>1</sup>*Department of Physics, Columbia University, New York, NY 10027*

<sup>2</sup>*Lawrence Berkeley National Laboratory, Berkeley, CA 94720*

<sup>3</sup>*Department of Physics and Astronomy, University of Alabama, Tuscaloosa, AL 35487*

<sup>4</sup>*Diablo Canyon Power Plant, Pacific Gas and Electric Company, Avila Beach, CA 93424 and*

<sup>5</sup>*Physics Department, Stanford University, Stanford, CA 94305*

(Dated: February 5, 2018)

Anti-neutrino emission rates from nuclear reactors are determined from thermal power measurements and fission rate calculations. The uncertainties in these quantities for commercial power plants and their impact on the calculated interaction rates in  $\bar{\nu}_e$  detectors is examined. We discuss reactor-to-reactor correlations between the leading uncertainties, and their relevance to reactor  $\bar{\nu}_e$  experiments.

PACS numbers: 13.15.+g, 14.60.Pq, 28.41.-i

## I. INTRODUCTION

Electron anti-neutrinos from large commercial nuclear reactors are playing an important role in the exploration of neutrino oscillations [1]. The choice of distance between source and detector allows one to conveniently tune an experiment's sensitivity to either the atmospheric or solar neutrino mass splitting. KamLAND [2, 3, 4] has established a connection between the MSW effect in the sun [5] and vacuum oscillations with anti-neutrinos, and has provided the most accurate measurement of  $\Delta m_{21}^2$  to date. Earlier, CHOOZ [6] and Palo Verde [7] provided what are still the best upper limits on the mixing angle  $\theta_{13}$ . A variety of new experiments are being constructed to perform more sensitive measurements of the mixing angle  $\theta_{13}$  [8, 9, 10, 11, 12]. Anti-neutrino detectors at very short distance are being explored with the purpose of detecting coherent neutrino-nucleon scattering (C $\nu$ NS) [13], and for testing plutonium diversion at commercial reactors [14]. A proper understanding of the systematic effects involved in the modeling of the reactor anti-neutrino flux and energy spectrum is essential for these experiments. Moreover, as most experiments measure  $\bar{\nu}_e$ s from more than one reactor, it is important to understand not only the magnitude of these effects, but also the correlations between uncertainties from different sources.

Except for the case of C $\nu$ NS, which will not be addressed further here, reactor anti-neutrinos are usually detected using the inverse- $\beta$  reaction  $\bar{\nu}_e + p \rightarrow n + e^+$  whose correlated signature helps reduce backgrounds but is only sensitive to  $\bar{\nu}_e$ s with energy above 1.8 MeV. The kinetic energy of the positron gives a measure of the incoming  $\bar{\nu}_e$  energy. Neutrino oscillation parameters may be extracted from the data by fitting the observed  $\bar{\nu}_e$

spectrum  $\frac{dn_{\nu}}{dE_{\nu}}$  to the following equation:

$$\frac{dn_{\nu}}{dE_{\nu}} = \sum_k^{\text{reactors}} N_p \epsilon(E_{\nu}) \sigma(E_{\nu}) \frac{P_{ee}(E_{\nu}, L_k)}{4\pi L_k^2} S_k(E_{\nu}). \quad (1)$$

Here,  $N_p$  is the number of target protons,  $\epsilon(E_{\nu})$  is the energy-dependent detection efficiency,  $\sigma(E_{\nu})$  is the detection cross-section,  $P_{ee}(E_{\nu}, L_k)$  is the oscillation survival probability for  $\bar{\nu}_e$ s traveling a distance  $L_k$  from reactor  $k$  to the detector, and  $S_k(E_{\nu})$  is the  $\bar{\nu}_e$  spectrum emitted by reactor  $k$ . The time variation of the flux may be included in the fit to discriminate the time-varying reactor signal from constant backgrounds. Equation 1 should technically be multiplied by the detector resolution function and integrated over  $E_{\nu}$ , but this detail is inconsequential for our analysis.

Nuclear power reactors operate on the principle that the fission of U and Pu isotopes and the subsequent decays of their daughter fragments release energy, generating heat. Large Q-value  $\beta$ -decays of unstable fission fragments are primarily responsible for the  $\bar{\nu}_e$  emission of nuclear reactors. Decays of long-lived isotopes in the nuclear fuel and in spent fuel elements stored at the reactor site contribute at the sub-percent level to the detected  $\bar{\nu}_e$  flux; this contribution has been treated elsewhere [15] and is beyond the scope of this paper. Considering only fission reactions, the final term in Equation 1 may be expanded as

$$S(E_{\nu}) = \sum_i^{\text{isotopes}} f_i \left( \frac{dN_{\nu i}}{dE_{\nu}} \right), \quad (2)$$

where  $dN_{\nu i}/dE_{\nu}$  is the  $\bar{\nu}_e$  emission spectrum per fission of isotope  $i$ , and  $f_i$  is the number of fissions of isotope  $i$  during the data taking period. Since >99.9% of the energy- and  $\bar{\nu}_e$ -producing fissions are from  $^{235}\text{U}$ ,  $^{238}\text{U}$ ,  $^{239}\text{Pu}$ , and  $^{241}\text{Pu}$  [16] (see Figure 1), the summation in Equation 2 is performed over just these 4 isotopes. For  $^{235}\text{U}$ ,  $^{239}\text{Pu}$ , and  $^{241}\text{Pu}$ , the emitted  $\bar{\nu}_e$  spectra  $dN_{\nu i}/dE_{\nu}$  are derived from  $\beta$ -spectrum measurements of the fissioning of the isotopes by thermal neutrons [17, 18]. The uncertainty

\*Electronic address: zdjuric@nevis.columbia.edu

†Electronic address: JADetwiler@lbl.gov

‡Present address: Sierra Nevada Corp., Los Gatos, CA 95032

in the  $\bar{\nu}_e$  spectral shape derived from these measurements was investigated recently in [19]. For  $^{238}\text{U}$ , no measurements are available, so theoretical calculations of its  $\bar{\nu}_e$  emission must be used [20].

The  $f_i$  can be obtained from detailed simulations of the reactor core throughout the data taking period. The output  $f_i$  must obey the thermal energy constraint

$$W_{th} = \sum_{i=1}^{\text{isotopes}} f_i e_i, \quad (3)$$

where  $W_{th}$  is the total thermal energy produced by the reactor during the time period considered, and  $e_i$  denotes the energy released per fission of isotope  $i$ . To reduce sensitivity to errors in the simulation codes, the codes are typically used to obtain not the  $f_i$  directly but the fission fractions  $f_i/F$ , where  $F = \sum_i f_i$ . Measurements of the total generated thermal power taken regularly during reactor operation may then be used to obtain the total numbers of fissions of each isotope using Equation 3.

The appropriate simulation codes are cumbersome to run, and are often proprietary, and therefore are not always available for direct use by scientific collaborations. Obtaining the  $f_i/F$  therefore requires special agreements with reactor operators. Depending on the terms of the agreement, fine grained time-dependent fission fractions may be obtained. Fine-grained data for  $W_{th}$  are commonly available, since such information must be made available to nuclear regulatory bodies. Reactor  $\bar{\nu}_e$  experiments then use this information to calculate the  $\bar{\nu}_e$  signal using an equation of the following form:

$$n_\nu = \frac{W_{th}}{\sum_i (f_i/F) e_i} \sum_{i=1}^{\text{isotopes}} \left( \frac{f_i}{F} \right) n_i, \quad (4)$$

where for simplicity we have assumed a single reactor, and have integrated over  $E_\nu$ . The terms in Equations 1 and 2 not appearing in Equation 4 have been grouped into the  $n_i$ , the number of detected  $\bar{\nu}_e$  per fission of isotope  $i$ .

Most recent reactor  $\bar{\nu}_e$  experiments, including KamLAND [2, 3, 4], CHOOZ [6], Palo Verde [7] and Bugey [21], have used Equation 4, or variations on it, to perform their signal calculations. In the first two experiments, the systematic uncertainty in the signal calculation was taken to be the quadratic sum of the uncertainty in the reactor power measurements which yield  $W_{th}$  and some estimate of the error due to the uncertainty in the fission fractions  $f_i/F$ . In the case of Palo Verde this latter component was estimated from comparisons between calculated and measured isotopic concentrations in spent fuel elements [16]. In the case of KamLAND this component was taken from comparisons of a simplified reactor model to detailed simulations [2, 3, 4, 22], which assumes that the uncertainty of the simplified reactor model significantly exceeds that of the detailed simulations. However, no systematic uncertainty was assigned to the detailed reactor simulations. The CHOOZ experiment [6]

leveraged the short baseline Bugey observation to limit the reaction cross section uncertainty, scaling their result to agree with the Bugey-measured cross section per fission. This treatment allowed CHOOZ to significantly reduce the error associated with the  $\bar{\nu}_e$  emission spectra ( $dN_\nu/dE_\nu$ ). However, their method is legitimate only to the extent that the reactor simulations employed by the CHOOZ and Bugey reactor operators reliably model the different reactors with their specific fuel compositions and operation histories. In all cases, the combined systematic error was estimated to be within 2-3%. At this level, the different methods employed by each experiment are likely not overly aggressive.

With detector-based uncertainties in current and next-generation reactor  $\bar{\nu}_e$  experiments approaching the  $\sim 1\%$  scale, a more careful treatment of these reactor-specific uncertainties is necessary, particularly for experiments with multiple reactor sources in which correlations become important. In this paper we outline such a detailed treatment of these uncertainties and demonstrate its application to a counting analysis of  $\bar{\nu}_e$ 's from single and multiple commercial reactor sources. In Section II we discuss in detail the uncertainty in reactor thermal power measurements. In Section III we examine the Monte-Carlo estimation of the  $f_i$  and, expanding on the treatment in [16] and [23], derive uncertainties for these based on a large body of spent fuel isotopic concentration comparisons used to verify the codes. In Section IV we combine the uncertainties from  $W_{th}$  and the  $f_i$  to estimate their contribution to the uncertainty in the anti-neutrino yield. We also discuss the applications of our calculation to specific experimental configurations, including multiple reactor sources. We draw our conclusions in Section V.

Our analysis addresses issues common to large commercial power reactors, especially Pressurized-Water-Reactors (PWRs) and Boiling-Water-Reactors (BWRs), using low-enrichment fuel. Explanation of the operation of PWRs and BWRs may be found in [24]. Modern neutrino experiments are almost exclusively using  $\bar{\nu}_e$  from such reactors. Minor contributions from other reactor types are not considered here. All uncertainties are given at the 68.3% confidence level.

## II. THERMAL POWER UNCERTAINTY

The most accurate measurement of a reactor's thermal power is given by a calculation of the energy balance around the reactor vessel (BWR) or steam generator (PWR). This requires accurate measurements of feed-water mass flow and temperature, steam enthalpy and moisture content, and reactor coolant-cycle heat gains and losses [25]. For the PWRs at Diablo Canyon Power Plant (DCPP) (California, USA), the thermal balance is written as

$$Q_C = Q_S + Q_{LTND} + Q_{R\&C} - Q_{RCP} - Q_{PZ}. \quad (5)$$

$Q_C$  is the core thermal output, the time-integral of which gives  $W_{th}$ . The largest component of it,  $Q_S$ , is the power extracted from the steam produced directly in the steam generator. Smaller corrections are represented by:  $Q_{LTND}$ , the power lost in the water clean-up system;  $Q_{R\&C}$ , the power losses to the external environment due to radiation and convection;  $Q_{RCP}$ , the contribution to  $Q_S$  from heating of the working fluid by the circulation pumps; and  $Q_{PZ}$ , the contribution to  $Q_S$  from heating of the working fluid by the pressurizers. The correction terms together account for 0.3-0.4% of the total  $Q_C$ .

A similar thermal balance may be written for other PWRs as well as for BWRs. In the case of BWRs, the main component is also in the form of steam produced by the reactor. For both reactor types,  $Q_S$  is evaluated according to

$$Q_S = m_s (h_{out} - h_{in}), \quad (6)$$

where  $m_s$  is the mass flow rate of the feed-water to the steam generator (PWR) or reactor vessel (BWR), and  $h_{out} - h_{in}$  is the specific enthalpy rise in the steam generation. We will discuss the uncertainties in these terms below. The uncertainties on the terms other than  $Q_S$  in the thermal balance equation (Equation 5) contribute negligibly to the uncertainty of the core thermal power and will not be addressed further here.

The enthalpy rise is calculated, using steam tables [26], from inlet and outlet values of the pressure and temperature, and from the moisture content on the secondary side of the steam generator or reactor vessel. The enthalpy uncertainty has several contributions deriving from measured and calculated quantities. The errors in the temperature and pressure measurements are assumed to be random after correction for known systematic contributions. The moisture content of the steam is generally known to grow during the operation cycle because of reduced moisture removal efficiency of the steam separators due to a slow deposition of eroded metal particles. The moisture content uncertainty of the steam may be treated as a systematic uncertainty since all reactors undergo this aging process. The calculation of the enthalpy rise from these inputs using steam tables contributes an additional systematic uncertainty of <0.2% [27].

As an example, Table I shows the uncertainties of the quantities relevant to the enthalpy calculation for DCP. The moisture content at DCP's steam generators grows with time, as mentioned above; the number in Table I is an average over the period of operation. Over longer periods the moisture content may grow, as explained above, by a factor of two over the level represented in Table I, but even then it will comprise a sub-dominant contribution to the error budget. A similar analysis for Beaver Valley Unit 2 yielded enthalpy-related contributions to the thermal power uncertainty totaling 0.16% [28]. A more general discussion in [29] uses an enthalpy uncertainty of 0.24%. For a generic reactor or when a more detailed analysis is unavailable, we suggest conservatively assuming 0.15% random uncertainty (for the  $p$  and  $T$

TABLE I: Uncertainty contribution to the enthalpy from measured input quantities at DCP. The change of the enthalpy vs given quantity, ( $\Delta$ Enthalpy/ $\Delta$ Quantity), is calculated using steam tables [26].  $p_{in}$ ,  $T_{in}$  and  $p_{out}$  are the inlet pressure, the inlet temperature, and the outlet pressure, respectively. The present moisture carryover value at DCP is assumed in the table. The quadratic sum conservatively assumes a full 0.2% error related to the use of steam tables to calculate the enthalpy rise.

Quantity	Typical Value	Quantity Error [%]	$\frac{\Delta$ Enthalpy $\Delta$ Quantity	Enthalpy Error [%]
$p_{in}$	6.9 MPa	0.50	0.002	0.001
$T_{in}$	221 °C	0.12	1.153	0.138
$p_{out}$	5.6 MPa	0.94	0.018	0.017
Moisture content	0.99	0.05	0.562	0.028
Steam tables				<0.2
Quadratic Sum				0.25

measurements) and 0.2% systematic uncertainty (due to the moisture content and use of steam tables) for the enthalpy rise.

The uncertainty in  $m_s$  gives the largest contribution to the error in the thermal power [30, 31]. In order to provide as accurate a measurement as possible, the flow rate is measured in a long, straight section of pipe where fully developed turbulent flow is established. Different types of flow meters may be employed there. Traditionally the system is instrumented with nozzle-based flow meters operating on the principle of the Venturi effect. An early analysis yielded a total flow uncertainty for these meters of 1.7%, of which 1.6% is attributable to random errors, while the systematic uncertainty is determined to be 0.5% [32]. According to more recent experience at DCP, properly calibrated and maintained Venturi meters can be operated with an initially low total uncertainty of about 0.7%. However, the accuracy of the Venturi meters fluctuates with time due to material deposition, or "fouling" [30], which leads to smaller cross sectional area for the flow through the device and results in indicated flow rates exceeding the true value. Depending upon the nozzle style and the pH factor of the feed-water, this fouling can grow as high as 3% over periods of a few months to a few years. In-situ comparisons between Venturi meters and more modern instrumentation (discussed below) shows an average systematic difference of +0.6%, and a statistical spread of ~1.4% [33, 34].

Fouling in Venturi flow meters results in economic losses for the nuclear power industry. Nuclear reactor regulations in the US and elsewhere require operators to apply a safety margin accounting for the uncertainty in the thermal power measurement when performing loss-of-coolant accident and emergency core cooling system performance analyses. However, the regulatory practice varies from country to country [35]. The size of the safety margin is 2% in the US, but may be reduced if the thermal power measurement uncertainties can be demonstrated to be smaller than that level [36]. For reactors

instrumented with Venturi meters, for which lower uncertainties cannot be demonstrated as a result of fouling, this in effect leads to operation at 2% below the plant's licensed operating power limit. A similar 2% safety margin is required in Japan [37]. Moreover, fouling itself results in an overestimation of the thermal power, leading to actual operation up to a few percent below the indicated level, and thus a lower electric power output. This two-fold impact of fouling gives the nuclear power industry a high incentive to deploy a replacement technology with smaller, well-understood uncertainties.

Using a new generation of ultrasonic flow meters (UFM) not affected by fouling, the thermal power uncertainty may be significantly reduced. UFM's use an electronic transducer with no differential pressure elements. There are currently two types of UFM systems routinely used in the nuclear electric generation industry to accurately calculate feed-water flow in high purity water [38]. One style is the transit-time meter, while the other is the cross-flow meter. The transit-time UFM emits ultrasound signals diagonally through the fluid upstream and downstream along the same path. The measured time difference between the two paths is proportional to the velocity of the fluid in the pipe. Accuracies of 0.2-0.5% are reported [39, 40] for transit-time type UFM's. The cross-flow UFM measures the time taken by a unique pattern of turbulent eddies in the fluid to travel between two pairs of transducers at some known distance apart along the pipe. The cross-flow devices are mounted externally to the pipe. The cross-flow UFM with its associated hardware and software is able to achieve a flow measurement uncertainty of 0.25% or better, although the ability to achieve these uncertainties in real reactor conditions has been questioned [41]. This type of meter is employed at DCP, with an uncertainty evaluated in-situ within the 0.4-0.7% range. The principles of operation of both transit-time and cross-flow UFM's are described in detail in [42].

The measurement uncertainties of transit-time UFM's and their breakdown into statistical and systematic components were studied in detail by Estrada [40] of Caldon Inc., a flow meter manufacturer for the nuclear industry. This work found total uncertainties in the measured mass flow rates of 0.45% for models with externally mounted transducers, and 0.20% for intrusive-type models with 4 pairs of transducers. We refer to these as Type I and Type II UFM's, respectively. These uncertainties originate from the differences between the water axial velocity profile in the test facility and in the measurement system in a plant, the uncertainty in the measurement of the ultrasound acoustic path in the water pipe, the imperfect knowledge of the dimensions of the measurement systems, and the uncertainty in the measurement of the time of flight of the acoustic pulses, including non-fluid delays. The water flow uncertainties are divided into random and systematic contributions in Table II.

We note that the 0.45% uncertainty based on Estrada's study is consistent with the 0.4-0.7% uncertainty esti-

TABLE II: Typical flow meter uncertainties. Type I corresponds to transit-time (TT) UFM's with ultrasonic transducers externally mounted to the feed-water pipe. Type II corresponds to transit-time UFM's with ultrasonic transducers in-line with the pipe via a spool piece that integrates four pairs of ultrasonic transducers, forming four chordal paths. Type I-II UFM water flow uncertainties are based on Caldon Inc. experience [40]. The flow meter employed at DCP is of the cross-flow (CF) type.

Flow Meter	Random [%]	Syst. [%]	Total [%]
Venturi	1.4	0.6	1.5
Type I TT UFM	0.2	0.4	0.45
Type II TT UFM	0.09	0.18	0.20
DCP CF UFM	0.3-0.6	0.1-0.2	0.4-0.7

TABLE III: Typical thermal balance quantities for the Diablo Canyon PWR reactors.

Quantity	Typical Value	Error [%]
$m_s$	1887 kg/s	0.4-0.7
$\Delta h = h_{out} - h_{in}$	$1.819 \cdot 10^6$ J/kg	0.25
$Q_S$	3433 MWt	$\lesssim 0.7$
$Q_{LTND}$	1.83 MWt	nil
$Q_{R\&C}$	0.65 MWt	nil
$Q_{RCP}$	14 MWt	nil
$Q_{PZ}$	0.21 MWt	nil
$Q_C$	3421 MWt	$\lesssim 0.7$

ated by DCP for cross-flow meters. Several other assessments of mass flow rate uncertainties, also consistent with these values, may be found in the literature. The generic discussion in [29], for example, quotes feed-water flow uncertainties of 0.4%. For a generic UFM, we will use the values listed for the Type I transit-time UFM, which has the largest estimated systematic uncertainty, and gives a total error consistent with values considered by the US Nuclear Regulatory Commission in a discussion on the use of UFM's [41].

The errors on the enthalpy rise and  $m_s$  may be added in quadrature to obtain the full error on  $Q_S$ . Combining the mass flow uncertainty (as given in Table II for Type I transit-time UFM's) with an enthalpy uncertainty of 0.25%, we get a total thermal power uncertainty of 0.51%, of which 0.45% is systematic and 0.25% will vary from reactor-to-reactor. Typical values for the quantities describing the heat balance and their error are given in Table III for DCP, using two PRW's equipped with cross-flow type UFM's. An internal DCP study characterized about a quarter of the thermal power uncertainty as correlated. The error in the determination of  $Q_S$ , which is the only non-negligible component of  $Q_C$  and hence determines the uncertainty on  $W_{th}$ , is dominated by the uncertainty in  $m_s$ . For precise evaluation of the errors, the enthalpy uncertainty has to be taken into account.

It is worth mentioning that most feed-water flow applications require two or more flow measurements. In

PWRs, for example, the flow is measured in each steam generator. In BWRs, the flow is normally measured in each of two main feed headers. In these cases, the random uncertainties may be reduced by a factor of  $1/\sqrt{\text{number of generators}}$  or  $1/\sqrt{2}$ , respectively.

It is also worth noting that estimates of flow rate measurement uncertainties to date have been performed in laboratory settings at Reynolds numbers of up to  $10^6$ . However, Reynolds numbers in actual power plants are as high as  $10^7$  [29, 43, 44]. The uncertainty estimates described above are therefore extrapolations from the lower Reynolds number evaluations. Although the error associated with these extrapolations is expected to be small, new test facilities have been proposed to generate realistic flow conditions with a higher Reynolds number to test these extrapolations [45].

### III. UNCERTAINTIES IN FISSION CALCULATIONS

During the power cycle of a nuclear reactor, the composition of the fuel changes as Pu isotopes are bred and U is depleted. At the end of the power cycle, some fraction of the fuel is replaced, and the remaining fuel elements are shuffled to optimize burnup. Knowledge of the detailed, time-dependent radionuclide content of the spent fuel throughout the power cycle is of interest to reactor operators and regulatory groups because it impacts shielding requirements, dose rate analysis, toxicity, waste storage and handling considerations, and criticality safety [46]. To obtain this knowledge, reactor operators employ Monte-Carlo simulations of the reactor core. The simulations begin with an initial fuel composition and a physical model of the core assembly. An initial neutron flux solution for the core is computed based on a number of inputs, including the measured thermal power generation, and other operating parameters such as the pressure, temperature, and flow rate of the cooling system, neutron moderation parameters, etc. Cross-section and decay data libraries are used to compute the rate of various interactions and update the fuel composition as a function of position. This process is iterated in a series of time-steps throughout the reactor power cycle.

As a by-product, these reactor core simulations may be made to output the number of fissions  $f_i$  needed for the estimation of the signal in reactor anti-neutrino experiments. A plot of the time-dependent fission rates calculated for a typical power cycle of one of the reactors at the Palo Verde Nuclear Generating Station (PVNGS) in Arizona, USA, is shown in Figure 1. Integrating over the power cycle gives the  $f_i$  required by Equation 4 to compute the  $\bar{\nu}_e$  signal.

Uncertainties in these simulation codes originate from a variety of sources [47]. These sources include the uncertainties in the input parameters, uncertainties in the nuclear cross-section and decay data used by the codes, approximations made in the modeling of the reactor core,

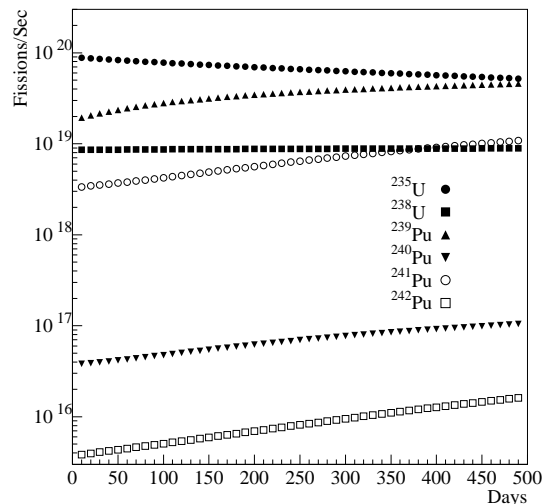


FIG. 1: Fission rates for various isotopes during a typical 500 day fuel cycle for one of the Palo Verde Nuclear Generating Station reactors in Arizona (USA).  $>99.9\%$  of the  $\bar{\nu}_e$ s are emitted by  $^{235}\text{U}$ ,  $^{238}\text{U}$ ,  $^{239}\text{Pu}$ , and  $^{241}\text{Pu}$  [16].

and numerical approximations used in the computations themselves. Reference [16] explored the input parameter uncertainty contribution with the reactor core simulation code used at PVNGS [48, 49] by calculating the  $\bar{\nu}_e$  signal variation for a given deviation of several of the input parameters. For the PVNGS simulation, the normalization to the measured thermal power represented by Equation 4 was done within the code. The code was run for a set of 500-day power cycles with one parameter varied at a time. The results of the study are shown in Figure 2. The thermal power measurement has the largest effect, with a slope of 0.96.

The most common means reactor operators use to globally assess the performance of the codes is to compare measurements of the isotopic content of spent fuel elements with the values predicted by the simulations. Such verifications have been performed for a number of codes at a variety of PWRs and BWRs in the US, Japan and Europe [50, 51, 52, 53]. Samples are obtained from representative locations throughout the core, commonly selected from regions that are difficult to simulate accurately, such as boundaries and hot-spots. The assay technique employed is typically isotopic dilution mass spectroscopy, for which errors of 1-3% are typical for the isotopes of interest [54]; in more recent measurements, errors below 0.3% have been achieved [46].

Figure 3 shows an example comparison between measured and calculated concentrations, in kilogram per metric tonne uranium (kg/MTU), of  $^{235}\text{U}$ ,  $^{238}\text{U}$ ,  $^{239}\text{Pu}$  and

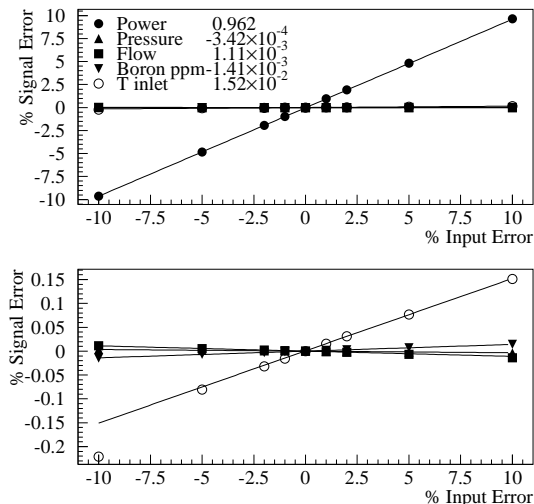


FIG. 2: The change in the expected  $\bar{\nu}_e$ -signal as a function of five inputs to the core simulation, taken from [16]. The numbers in the key are slopes of the fitted lines. The lower panel zooms in on the non-power inputs so that their variation can be observed.

$^{241}\text{Pu}$  as a function of burnup for a set of fuel elements processed at a typical PWR [46]. The quantity “burnup” in the abscissa is defined as the amount of energy (in GigaWatt days) extracted from a fuel element per unit initial mass of uranium (in MTU). The burnup is measured to within  $\sim 3\%$  for each sample using the  $^{148}\text{Nd}$  method [55], in which the integral number of fissions, determined from the sum of the  $^{148}\text{Nd}$  fission product yields for the four isotopes of interest, is multiplied by the average energy released per fission, weighted according to the calculated fission fractions. During a typical reactor cycle, fuel elements near the center of the reactor core receive a higher burnup than those at the edges, due to the higher neutron flux at the center. This spatial variation, along with the number of cycles over which the samples were processed, is responsible for the different burnup values achieved in the samples plotted in Figure 3. During normal operations, fuel elements are processed over several power cycles, and are shuffled between each power cycle, until optimal burnup is reached for all fuel elements. In practice, burnups up to  $\sim 50$  GWd/MTU are achieved in the typical operation of modern commercial reactors [56].

Fractional differences in the heavy isotope concentrations  $\delta c_i/c_i$  were calculated from the measured ( $M$ ) and calculated ( $C$ ) concentrations using the following sign

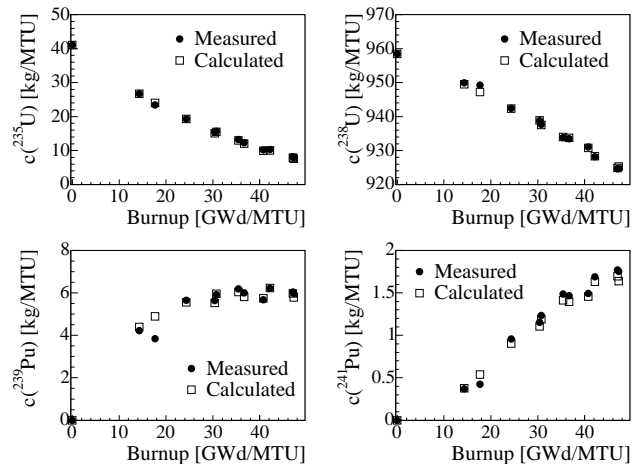


FIG. 3: Measured vs. calculated concentrations of  $^{235}\text{U}$ ,  $^{238}\text{U}$ ,  $^{239}\text{Pu}$  and  $^{241}\text{Pu}$  as a function of burnup for fuel elements taken from the Takahama Unit 3 PWR [46]. See the text for a definition of the units.

convention:

$$\frac{\delta c}{c} = \frac{c_C - c_M}{c_M}. \quad (7)$$

In Figure 4 we plot the values of  $\delta c_i/c_i$  ( $i = ^{235}\text{U}$ ,  $^{238}\text{U}$ ,  $^{239}\text{Pu}$ ,  $^{241}\text{Pu}$ ), using 159 comparisons of fuel element samples taken from ten PWRs and BWRs, modeled by a variety of core simulation codes. Details of the codes and reactors included in our analysis are listed with their references in Table IV. Gaussian fits to the distributions are drawn for reference. The individual distributions for PWRs and BWRs (not shown) are equivalent within the available statistics. The concentration comparisons also do not exhibit a strong trend with burnup, as shown in Figure 5.

Unfortunately, these isotopic concentration comparisons only give indirect information on the uncertainty in the number of fissions. However, we can estimate  $\delta f_i/f_i$  from  $\delta c_i/c_i$  by considering the nuclear processes responsible for the changes in isotopic concentrations through the lifetime of a typical fuel element. The U isotopes are the most straightforward to diagnose, since U breeding processes are negligible compared to U depletion processes. The decrease of the U concentrations with burnup results from a combination of fission and isotopic conversions due to other nuclear processes (e.g. n capture). The error on the total loss of U is the fractional error in the change in concentration after burnup  $B$ . We conservatively assign the error on the total loss of U entirely to fission processes, so that the fractional error on the number of U fissions is at most

$$\frac{\delta f_{\text{U}}}{f_{\text{U}}} = \frac{\delta(c_{\text{U}}(0) - c_{\text{U}}(B))}{c_{\text{U}}(0) - c_{\text{U}}(B)}, \quad (8)$$

where  $c_{\text{U}}(0)$  and  $c_{\text{U}}(B)$  are, respectively, the initial and final concentrations of either U isotope after burnup  $B$ .

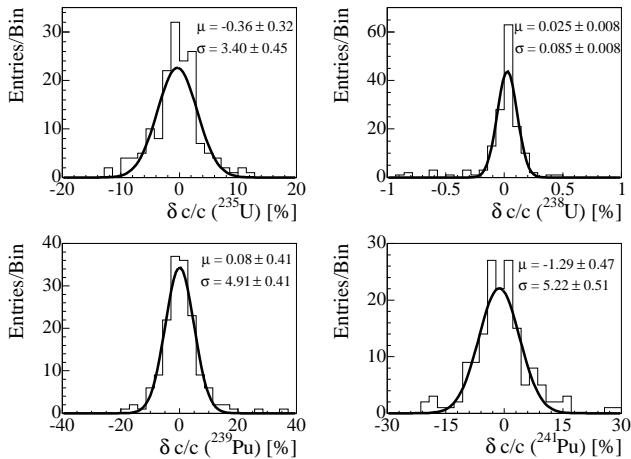


FIG. 4: The values  $\delta c/c$  for  $^{235}\text{U}$ ,  $^{238}\text{U}$ ,  $^{239}\text{Pu}$  and  $^{241}\text{Pu}$ , calculated for each of the 159 comparisons of fuel element samples taken from a number of PWRs and BWRs modeled by a variety of core simulation codes [46, 57, 58, 59, 60, 61].

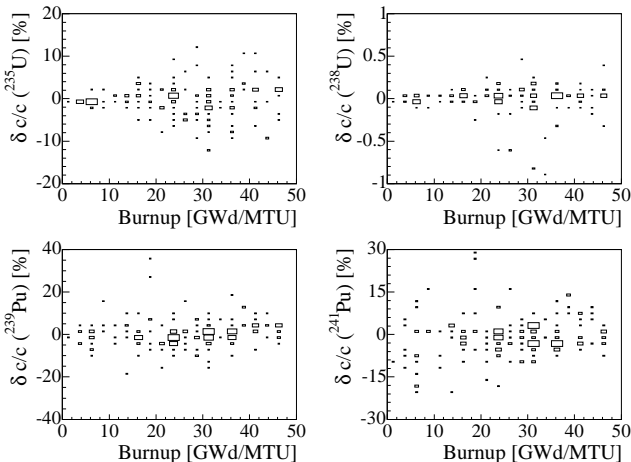


FIG. 5: The values  $\delta c/c$  for  $^{235}\text{U}$ ,  $^{238}\text{U}$ ,  $^{239}\text{Pu}$  and  $^{241}\text{Pu}$  as a function of burnup, calculated for each of the 159 fuel sample comparisons.

The initial  $^{235}\text{U}$  and  $^{238}\text{U}$  concentrations ( $c_U(0)$ ) are determined by the enrichment level of the fuel elements under consideration and are known very precisely. Hence the uncertainty  $\delta(c_U(0) - c_U(B))$  is dominated by the uncertainty in  $c_U(B)$ , allowing us to approximate

$$\frac{\delta f_U}{f_U} \approx - \left( \frac{1}{c_U(0)/c_U(B) - 1} \right) \frac{\delta c_U(B)}{c_U(B)}, \quad (9)$$

where the last term is the  $\delta c/c$  plotted in Figure 4. As can be seen in Figure 3, which is typical for fuel processed in commercial PWRs and BWRs, the factor in parenthesis in Equation 9 is significantly different from one for  $^{238}\text{U}$  but not for  $^{235}\text{U}$ , except at low burnup.

For the Pu isotopes the relationship between the

TABLE IV: Codes and reactors included in our analysis. In cases where multiple tests were performed on the same code/reactor using older cross section files or neglecting some reactor configuration or operation details, we used the comparisons for the most up-to-date data libraries and most detailed reactor model.

Ref.	Reactor (Type)	$W_{\text{th}}$ [MWt]	Code
[46]	Takahama Unit 3 (PWR)	2652	SAS2H HELIOS
[57]	Calvert Cliffs Unit 1(PWR) H.B. Robinson Unit 2 (PWR)	2560 2192	SCALE/SAS2H
[58]	Cooper (BWR) Gundremmingen (BWR) JDPR (BWR)	2381 801 45	SAS2H
[59]	Trino Vercellese (PWR) Turkey Point Unit 3 (PWR)	825 2300	SAS2H
[60]	San Onofre (PWR)	1347	SAS2H
[61]	Takahama Unit 3 (PWR) Fukushima Unit 2 (BWR)	2652 3293	SWAT ORIGEN2 SWAT ORIGEN2
[62]	Calvert Cliffs Unit 1(PWR)	2560	ORNL-Assm

TABLE V: Means ( $\mu$ ) and standard deviations ( $\sigma$ ) of  $\delta f_i/f_i$  for commercial reactors.

Fuel	$\mu$ [%]	$\sigma$ [%]
$^{235}\text{U}$	$0.09 \pm 0.16$	2.0
$^{238}\text{U}$	$-0.81 \pm 0.38$	4.8
$^{239}\text{Pu}$	$0.74 \pm 0.45$	5.7
$^{241}\text{Pu}$	$-0.32 \pm 0.48$	6.0

$\delta f_{\text{Pu}}/f_{\text{Pu}}$  and the  $\delta c_{\text{Pu}}/c_{\text{Pu}}$  is complicated by the presence of significant breeding processes. However, the sources of uncertainty in  $\delta f_{\text{Pu}}/f_{\text{Pu}}$  are the same as those in  $\delta c_{\text{Pu}}/c_{\text{Pu}}$ , indicating a similar magnitude. Moreover, since the Pu concentrations in fresh fuel used at typical commercial reactors starts at “zero” and the fission rate is at all values of  $B$  proportional to the concentration  $c_{\text{Pu}}(B)$ , we simply assume that  $\delta f_{\text{Pu}}/f_{\text{Pu}} \approx \delta c_{\text{Pu}}/c_{\text{Pu}}$  directly.

The four values of  $\delta f_i/f_i$  ( $i = ^{235}\text{U}, ^{238}\text{U}, ^{239}\text{Pu}, ^{241}\text{Pu}$ ) were calculated for each of the 159 comparisons of fuel element samples from the reactors and core simulation codes listed in Table IV, using Equation 9 for the U isotopes and letting  $\delta f_{\text{Pu}}/f_{\text{Pu}} \approx \delta c_{\text{Pu}}/c_{\text{Pu}}$  for the Pu isotopes. The means and standard deviations of the distributions for each isotope were extracted from Gaussian fits. The results are listed in Table V. Note that with our sign convention defined in Equation 7, a positive  $\delta f_i/f_i$  corresponds to an over-estimated fission count by the reactor core simulations.

Correlations between the  $\delta f_i/f_i$  were studied as well. Figure 6 plots the  $\delta f_i/f_i$  for pairs of fuel isotopes for

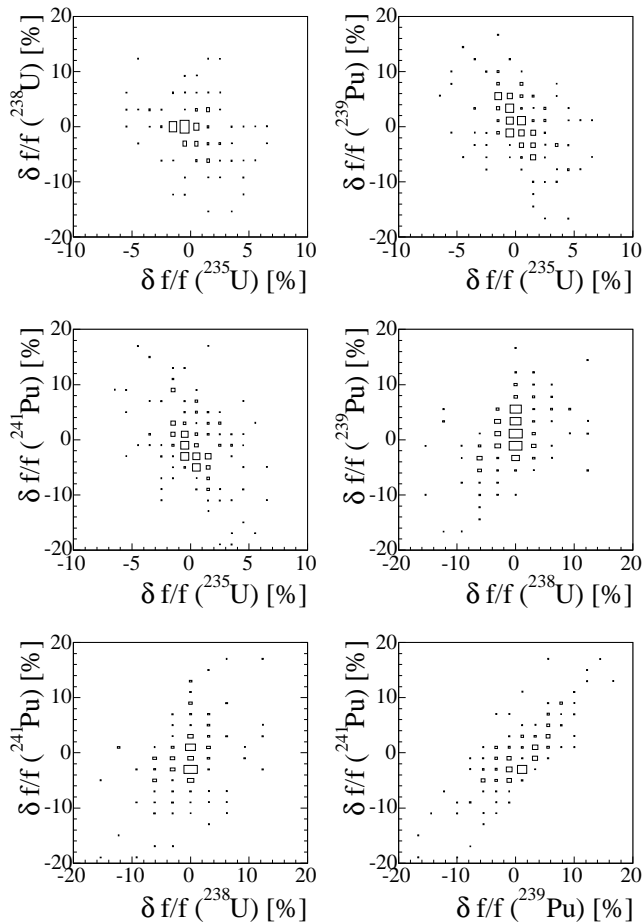


FIG. 6:  $\frac{\delta f_i}{f_i}$  dependencies for  $^{235}\text{U}$ ,  $^{238}\text{U}$ ,  $^{239}\text{Pu}$ , and  $^{241}\text{Pu}$ .

TABLE VI: Correlation coefficients  $\alpha_{ij}$  obtained from 2-dimensional Gaussian fits applied to the distributions from Figure 6

	$^{235}\text{U}$	$^{238}\text{U}$	$^{239}\text{Pu}$	$^{241}\text{Pu}$
$^{235}\text{U}$	1	-0.29	-0.62	-0.48
$^{238}\text{U}$	-0.29	1	0.38	0.39
$^{239}\text{Pu}$	-0.62	0.38	1	0.84
$^{241}\text{Pu}$	-0.48	0.39	0.84	1

all 159 fuel samples comparisons. Correlation coefficients  $\alpha_{ij}$  are obtained by fitting these distributions to 2-dimensional Gaussians:

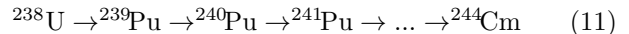
$$G(\Delta_i, \Delta_j) = A e^{-\frac{1}{2} \frac{1}{1-\alpha_{ij}^2} (\Delta_i^2 + \Delta_j^2 - 2\alpha_{ij} \Delta_i \Delta_j)}, \quad (10)$$

where  $\Delta_i \equiv (\delta f_i / f_i - \mu_i) / \sigma_i$  and  $A$  is a normalization constant. In the fit,  $\mu_i$  and  $\sigma_i$  are allowed to float, resulting in fit values consistent in all cases with the values listed in Table V. The fit values of  $\alpha_{ij}$  are listed in Table VI.

We find a weak anti-correlation between  $^{235}\text{U}$  and all of the other isotopes. This is expected since  $^{235}\text{U}$  dominates the thermal power production of the reactor, and so to

maintain the energy balance, the over-fissioning of this isotope must be accompanied by an under-fissioning of the other isotopes (and vice-versa). The fact that the largest anti-correlation is with  $^{239}\text{Pu}$ , the next largest energy producing heavy isotope after  $^{235}\text{U}$ , strengthens this argument.

We also find a strong correlation between the two Pu isotopes, which can be explained by the fact that  $^{239}\text{Pu}$  is a precursor to  $^{241}\text{Pu}$  in one of three main isotope transformation chains within the reactor core [63]:



Since there is little or no Pu in a fuel element at zero burnup, over-fissioning of a Pu isotope is associated with its overproduction in the simulation via this isotope transformation chain. If one Pu isotope is overproduced, it is likely that the other will also be overproduced, resulting, in more fissions from both isotopes.

The correlation between  $^{238}\text{U}$  and Pu isotopes is a bit harder to diagnose. However,  $^{238}\text{U}$  is only a minor player in the thermal power production, comprising only  $\sim 10\%$  of the output, so a strong anti-correlation is not expected as it is for  $^{235}\text{U}$ . And while  $^{238}\text{U}$  is the parent of the transformation chain represented by Equation 11, that chain represents a series of neutron captures, whereas the correlations listed in Table VI correspond to fissions. The over-fissioning of  $^{238}\text{U}$  does not a-priori imply a greater neutron capture rate to produce more of the Pu isotopes (so that more are available to fission), and vice-versa. The true  $^{238}\text{U}$ -Pu correlation is a combination of these competing effects.

#### IV. UNCERTAINTY IN THE ANTI-NEUTRINO SIGNAL CALCULATION

We now examine how to propagate the uncertainties in  $W_{th}$  and the  $f_i$ , found in the previous sections, into the anti-neutrino signal uncertainty. This is not straightforward because of the significant correlation between  $\delta W_{th}$  and the  $\delta f_i$ , as indicated by Equation 3. To first order, an increase in the thermal power by some factor implies an increase in the  $f_i$  by the same factor. In fact, if we use the  $\delta f_i / f_i$  obtained from each spent fuel element discussed in the previous section to extract the thermal power uncertainty via standard error propagation on Equation 3, we obtain a distribution of  $\delta W_{th} / W_{th}$  with width 2.5%, consistent with the expectation for a set of reactors instrumented with Venturi-type flow meters of varying ages.

The point of the thermal power normalization in Equation 4 is to break this first-order correlation between the  $f_i$  and  $W_{th}$ , and work with the fission fractions  $f_i / F$  rather than the bare  $f_i$ . But even the  $f_i / F$  have a residual correlation with the thermal power that is due to the fact that U isotopes are depleted while Pu isotopes are bred during reactor operation. An over-estimate of the power will lead to an over-estimate of the Pu production, and hence a higher estimated fraction of fissions from the



Pu isotopes. This is significant for the  $\bar{\nu}_e$  signal estimation because, by coincidence, the  $e_i$  are slightly higher and the  $n_i$  are slightly lower for the Pu isotopes than for the U isotopes. Since the  $e_i$  appear in the denominator of Equation 4 and the  $n_i$  appear in the numerator, the effect is to lower slightly the signal estimate.

Hence we see that the contributions to the signal uncertainty from the errors on  $W_{th}$  and the  $f_i/F$  are slightly anti-correlated. It is this anti-correlation that is responsible for the slope of “Power” in Figure 2 being slightly less than one. However, the anti-correlation is only slight, and moreover implies a weak cancellation between the uncertainty contributions evaluated from the independent variation of  $W_{th}$  and the  $f_i/F$ . To maintain simplicity in our analysis while remaining conservative in the error propagation, we ignore this anti-correlation and treat the errors due to these terms as being uncorrelated. We thus evaluate the uncertainty on the  $\bar{\nu}_e$  signal,  $\sigma_\nu$ , according to the simple quadratic sum of contributions from each of the terms appearing in Equation 4:

$$\sigma_{n_\nu}^2 = \sigma_W^2 + \sigma_f^2 + \sigma_e^2 + \sigma_{other}^2. \quad (12)$$

Since Equation 4 is linear in  $W_{th}$ , the first term,  $\sigma_W$ , is given by the thermal power uncertainty,  $\delta W_{th}/W_{th}$ , discussed in detail in Section II. The contribution  $\sigma_f$  from the fission calculation uncertainties,  $\delta f_i/f_i$  is more complex and will be described below. The third term,  $\sigma_e$ , is the contribution due to the uncertainty in the  $e_i$ . The last term,  $\sigma_{other}$ , represents uncertainties in detector-specific components and other terms (such as the  $dN_\nu/dE_\nu$ ) that have been explored elsewhere. This term will not be addressed further here.

Before addressing  $\sigma_f$ , we briefly note that  $\sigma_e$  can be evaluated from error propagation on Equation 4. Assuming that the errors on each of the  $e_i$  are uncorrelated, we obtain

$$\sigma_e^2 = \frac{\sum_i (f_i/F)^2 \delta e_i^2}{[\sum_i (f_i/F) e_i]^2} \quad (13)$$

The values of the  $e_i$  and their uncertainties  $\delta e_i$  are given in [64, 65] as  $e(^{235}\text{U}) = 201.7 \pm 0.6$  MeV,  $e(^{238}\text{U}) = 205.0 \pm 0.9$  MeV,  $e(^{239}\text{Pu}) = 210.0 \pm 0.9$  MeV, and  $e(^{241}\text{Pu}) = 212.4 \pm 1.0$  MeV. To evaluate  $\sigma_e$ , we need to choose values for the fission fractions,  $f_i/F$ . As examples, Table VII shows the fission fractions for the three reactor units of PVNGS (PV1, PV2, and PV3), as well as averaged fission fractions of the reactors in Japan (KL), observed by the KamLAND experiment. The fission fraction values vary from reactor to reactor depending on the initial enrichment level and power history of the fuel. Table VII gives the corresponding value of  $\sigma_e$ , calculated with Eq. 13. In all cases considered, the value of  $\sigma_e$  is  $\sim 0.2\%$ .

Correlations between the  $\delta f_i/f_i$  make an analytical estimate of  $\sigma_f$  difficult. Instead we leverage the measured  $\delta f_i/f_i$  from Section III to compute, for each of the 159 spent fuel element comparisons, a value of  $\sigma_f$  according

TABLE VII: Fission fractions  $\frac{f_i}{F}$ ,  $\sigma_e$ , and  $\sigma_f$  for the three PVNGS reactors (PV1, PV2, PV3), and for all reactors viewed by KamLAND [3] (KL), averaged over the periods of operation.

Reactor or reactor group	$\frac{f_i}{F}$ [%]				$\sigma_e$ [%]	$\sigma_f$ [%]
	$^{235}\text{U}$	$^{238}\text{U}$	$^{239}\text{Pu}$	$^{241}\text{Pu}$		
PV1	58.0	7.4	29.2	5.4	0.217	$0.13 \pm 0.84$
PV2	54.4	7.5	31.8	6.3	0.216	$0.13 \pm 0.89$
PV3	57.7	7.4	29.2	5.7	0.216	$0.13 \pm 0.84$
KL	56.3	7.9	30.1	5.7	0.216	$0.14 \pm 0.88$

to

$$\begin{aligned} \sigma_f &\equiv \left( \frac{\delta n_\nu}{n_\nu} \right)_f \\ &= \frac{1 + \left( \sum_i \frac{f_i}{F} \frac{\delta f_i}{f_i} n_i \right) / \left( \sum_i \frac{f_i}{F} n_i \right)}{1 + \left( \sum_i \frac{f_i}{F} \frac{\delta f_i}{f_i} e_i \right) / \left( \sum_i \frac{f_i}{F} e_i \right)} - 1. \end{aligned} \quad (14)$$

This equation may be obtained by replacing the  $f_i$  in Equation 4 with  $f_i + \delta f_i$ , and  $n_\nu$  with  $n_\nu + \delta n_\nu$ . By substituting the 159 values of  $\delta f_i/f_i$  into Equation 14, we maintain the implicit correlations between different isotopes. And as explained above, the normalization by the thermal power removes the influence of the  $W_{th}$  uncertainty on the  $\bar{\nu}_e$  signal, so that  $\sigma_f$  accounts for the contribution from  $\delta f_i/f_i$  only. To compute the values of the  $n_i$  in Equation 14, we assume no oscillation (i.e. short  $L$ ) and an energy-independent efficiency above the inverse beta-decay threshold. For the  $f_i/F$  we use the same sets of values used to evaluate  $\sigma_e$  listed in Table VII.

An example  $\sigma_f$  distribution is drawn in Figure 7 using the fission fractions from [3], listed in the “KL” row of Table VII. When drawing the distribution of  $\sigma_f$ , we weight the value from each spent fuel element comparison according to its burnup to account for the fact that the higher-burnup samples near the center of the reactor contribute proportionally more to the  $\bar{\nu}_e$  signal than the lower-burnup samples near the core edges. The set of comparisons still includes a disproportionately large number of fuel elements from regions that are challenging for the simulation; by including all such samples we ensure a conservative estimate of  $\sigma_f$ . These problematic samples are responsible for the relatively large tails and the few outliers in the distribution. In order to incorporate these samples without letting them dominate the characterization of the distribution, we fit the distribution to a single Gaussian, and take the fit mean and standard deviation as estimates of the systematic and statistical components, respectively, of  $\sigma_f$ . We repeated this procedure for each of the four choices of the  $f_i/F$  listed in Table VII. As can be seen from these examples,  $\sigma_f$  is typically about 0.9%, of which  $\sim 0.1\%$  is correlated between different reactors.

For an experiment at a single reactor, unless the experimenters and reactor operators have gone to extremes

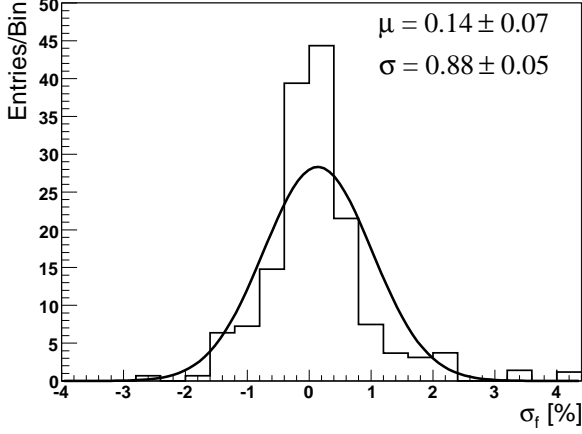


FIG. 7:  $\sigma_f$  distribution for the fuel comparisons, calculated with Eq. 14, weighted by sample burnup and fit to a Gaussian. The mean of the fit is identified as the systematic component of  $\sigma_f$ , while the spread represents the statistical uncertainty. The inclusion of a disproportionately large number of samples from regions that are challenging to simulate contributes larger tails and a higher mean, leading to more conservative estimates uncertainties.

to validate the core simulations, the uncertainty in the signal due to the error in the fission fraction calculations should be taken to be the full statistical uncertainty on  $\sigma_f$  added in quadrature with the systematic component. As an example, using the values listed in Table II with Type I transit-time UFM and incorporating the enthalpy uncertainties (as given in Table I) to obtain the thermal power uncertainty, the resulting uncertainty in the anti-neutrino yield, ignoring  $\sigma_{other}$ , is

$$\begin{aligned}
 \sigma_{n_\nu} &\approx \sqrt{\sigma_W^2 + \sigma_f^2 + \sigma_e^2} \\
 &\approx \sqrt{(0.2^2 + 0.4^2 + 0.15^2 + 0.2^2) + (0.14^2 + 0.9^2) + 0.2^2} \\
 &\approx 1.1\%.
 \end{aligned} \tag{15}$$

If the reactor instead measures the thermal power output at the 2% level, then this uncertainty evaluates to 2.2%.

For a multi-reactor experiment, some reduction of the statistical components of  $\sigma_W$  and  $\sigma_f$  is achieved. If reactor  $k$  contributes a fraction  $p_k$  to the total reactor  $\bar{\nu}_e$  signal, then the total random error in the summed signal is reduced by a factor of  $\sqrt{\sum_k p_k^2}$ . For example, consider the case of an experiment receiving an approximately equal signal from 2 reactors equipped with Type I transit-time UFMs. The resulting uncertainty in the anti-neutrino yield (again, ignoring  $\sigma_{other}$ ) is

$$\begin{aligned}
 \sigma_{n_\nu} &\approx \sqrt{\left(\frac{0.2^2}{2} + 0.4^2 + \frac{0.15^2}{2} + 0.2^2\right) + (0.14^2 + \frac{0.9^2}{2}) + 0.2^2} \\
 &\approx 0.83\%.
 \end{aligned} \tag{16}$$

TABLE VIII: Signal uncertainties at KamLAND,  $\sigma_\nu$ , obtained by combining  $\sigma_W$ , in quadrature with  $\sigma_f$  and  $\sigma_e$ . The calculations were performed assuming various power uncertainties. The 2.1% entry corresponds to the value used by the KamLAND collaboration.

$\sigma_W^{\text{single}}[\%]$	$\sigma_W[\%]$	$\sigma_f[\%]$	$\sigma_f^{MC}[\%]$	$\sigma_e[\%]$	$\sigma_{n_\nu}[\%]$
syst±stat	syst±stat	syst±stat			
2.10±0.00	2.10±0.00	0.14±0.18	1.0	0.216	2.3
0.60±1.40	0.60±0.26	0.14±0.18	0.2	0.216	0.76
0.45±0.25	0.45±0.05	0.14±0.18	0.2	0.216	0.59

As a more complex example, we study the thermal power and fission fraction uncertainties in the KamLAND experiment. We use the actual distance and nominal thermal power of the reactors to compute the fractions  $p_k$  they contribute to the signal [23]. We then allow all random uncertainties to be reduced by a factor of  $\sqrt{\sum_k p_k^2} \approx \frac{1}{5}$ . For the fission fraction uncertainty, the 0.88% statistical contribution for a single reactor is reduced to 0.18%. However, for KamLAND we must add an additional uncertainty,  $\sigma_f^{MC}$ , to account for the fact that to compute the fission fractions the KamLAND collaboration used a generic reactor simulation which was found to agree with detailed simulations, such as those considered in this paper, at the 1% level [22]. In this reference, this uncertainty appears to be dominated by random errors, so it may be appropriate to allow this component to also be reduced by a factor of  $\sim \frac{1}{5}$ .

For the thermal power uncertainty in the KamLAND example, we consider three scenarios: the standard KamLAND assumption of an across-the-board 2.1% systematic uncertainty, a slightly more realistic yet still conservative assumption that all Japanese reactors are equipped with properly-calibrated Venturi flow meters, and an ideal scenario in which all Japanese reactors are equipped with ultrasonic flow meters. The resulting values of  $\sigma_{n_\nu}^{\text{total}}$  are listed in Table VIII. For the standard KamLAND 2.1% thermal power error and with  $\sigma_f^{MC}$  taken to be the full 1%, the contributions of  $\sigma_f$  and  $\sigma_e$  are negligible, giving a result consistent with the 2.3% uncertainty used by the KamLAND collaboration, and justifying a classification of the KamLAND treatment as “conservative”. However, if we make the assumption that Japanese reactors are equipped with flow meters at least as performant as Venturi flow meters, and further take the spread in  $\sigma_f^{MC}$  evident in [22] to indicate that this term is predominantly random in nature, significant cancellations can be achieved. In this case, the systematic uncertainty due to the fouling is the dominant component; including all other components gives a total uncertainty of 0.76%. In an ideal scenario in which all Japanese reactors are equipped with Type I transit-time UFMs, the total uncertainty would drop to 0.59%. The dominant component is still the systematic uncertainty of the flow meter, but the relative contribution of the other terms is significant.

The actual situation in the Japanese reactor industry is

probably somewhere in between the all-Venturi case and the ideal case of all UFMs. Many reactors may already be equipped with UFMs, but some may not, and those that are may simply use them to calibrate their Venturi meters. However, the total uncertainty,  $\sigma_{n\nu}$ , does not change much between these two cases. Thus for KamLAND, a reduced error of 0.6-0.8% may be more appropriate. A better understanding of the nature of the Japanese instrumentation and reactor simulations may result in yet smaller overall uncertainties for KamLAND.

## V. CONCLUSION

The uncertainty in the estimated anti-neutrino interaction rate at reactor experiments has contributions from the thermal power and the fission calculation uncertainties. The dominant contributions to the thermal power uncertainty come from the enthalpy rise and mass flow rate in the steam generator (PWR) or reactor vessel (BWR). The former has a systematic uncertainty of 0.2% and a random uncertainty of typically 0.15%. The uncertainty in the mass flow rate depends on the instrumentation used to perform the measurement. Traditional Venturi flow meters exhibit significant fluctuations of 1.4% and a systematic uncertainty of 0.6% due to fouling. More precise ultrasonic flow meters have been evaluated to have systematic uncertainties below 0.5% and typically show random fluctuations below this level.

We estimated, for the first time to our knowledge, the contribution to the  $\bar{\nu}_e$  signal uncertainty from errors in the fission rate calculations. These errors were extracted from comparisons of heavy element concentration measurements in spent fuel elements with calculations of those concentrations by the same simulations that reactor  $\bar{\nu}_e$  experiments rely on to obtain the fraction of fissions from each of four main heavy isotopes. Error

propagation accounting for correlations between the four isotopes yielded a 0.1% systematic uncertainty on the  $\bar{\nu}_e$  signal rate, and a 0.9% random uncertainty. We also estimated a 0.2% contribution due to the uncertainty in the measured energy release per fission of each isotope.

We demonstrated how these errors can be combined for typical reactor experiment configurations, and highlighted situations in which cancellations occur between different reactor sites. With this methodology, we found that these contributions to the signal rate uncertainty in the KamLAND experiment may be reduced from 2.3% to 0.76%, or even 0.59%, pending better understanding of reactor instrumentation. As we move deeper into the phase of precision reactor neutrino oscillation experiments, and in particular multi-reactor  $\theta_{13}$  experiments, such sub-percent understanding of these errors and their systematic and random components will become more and more important. As reactor engineering, flow rate metrology, and core modeling continue to improve, further reductions may be achievable in these uncertainties. Toward this end, closer relationships between neutrino scientists and reactor operators should be encouraged.

## Acknowledgments

We are grateful to Harry Miley for providing some of the references used here and to Palo Verde Nuclear Generating Station for providing data used in the analysis. We thank Petr Vogel and Patrick Decowski for their careful reading and useful comments. We would also like to thank Akira Sebe and Kazuhiro Terao for their help in translating the Japanese references. This work was supported, in part, by U.S. National Science Foundation grant no. PHY-0758118, U.S. Department of Energy contract no. DE-AC02-05CH1123 and grant nos. DE-FG02-01ER41166 and DE-FG02-04ER41295.

- 
- [1] C. Bemporad, G. Gratta, and P. Vogel, *Rev. Mod. Phys.* **74**, 297 (2002); R. D. McKeown and P. Vogel, *Phys. Rept.* **394**, 315 (2004); G. L. Fogli *et al.*, *Prog. Part. Nucl. Phys.* **57**, 742 (2006); M. C. Gonzalez-Garcia and M. Maltoni, *Phys. Rept.* **460**, 1 (2008).
  - [2] K. Eguchi *et al.*, *Phys. Rev. Lett.* **90**, 021802 (2003).
  - [3] K. Eguchi *et al.*, *Phys. Rev. Lett.* **94**, 081801 (2005).
  - [4] S. Abe *et al.*, *Phys. Rev. Lett.* **100**, 221803 (2008).
  - [5] L. Wolfenstein, *Phys. Rev. D* **17**, 2369 (1978); S. P. Mikheyev and A. Y. Smirnov, *Sov. J. Nucl. Phys.* **42**, 13 (1985).
  - [6] M. Apollonio *et al.*, *Eur. Phys. J. C* **27**, 331 (2003).
  - [7] F. Boehm *et al.*, *Phys. Rev. D* **64**, 112001 (2001).
  - [8] K. Anderson *et al.*, hep-ex/0402041v1 (2004).
  - [9] F. Ardellier *et al.*, hep-ex/0606025v4, (2006).
  - [10] X. Guo *et al.*, hep-ex/0701029v1 (2007).
  - [11] J. C. Anjos *et al.*, *Nucl. Phys. Proc. Suppl.* **155**, 231 (2006).
  - [12] S. B. Kim *et al.*, <http://neutrino.snu.ac.kr/RENO> (accessed August 1, 2008).
  - [13] P. S. Barbeau, J. I. Collar, and O. Tench, *JCAP* **09**, 009 (2007).
  - [14] A. Bernstein *et al.*, *J. Appl. Phys.* **91**, 4672 (2002); A. Bernstein *et al.*, *J. Appl. Phys.* **103**, 074905 (2008).
  - [15] V. I. Kopeikin *et al.*, *Phys. Atom. Nuclei* **64**, 849 (2001).
  - [16] L. Miller, Ph.D. Thesis, Stanford University, 2001.
  - [17] K. Schreckenbach *et al.*, *Phys. Lett. B* **160**, 325 (1985).
  - [18] A. A. Hahn *et al.*, *Phys. Lett. B* **218**, 365 (1989).
  - [19] P. Vogel, *Phys. Rev. C* **76**, 025504 (2007).
  - [20] P. Vogel *et al.*, *Phys. Rev. C* **24**, 1543 (1981).
  - [21] Y. Declais *et al.*, *Phys. Lett. B* **338**, 383 (1994).
  - [22] K. Nakajima *et al.*, *Nucl. Instrum. Meth. Phys. Res. A* **569**, 837 (2006).
  - [23] Z. Djurcic, Ph.D. Thesis, University of Alabama, 2004.
  - [24] J. K. Shultis and R. E. Faw, *Fundamentals of Nuclear Science and Engineering* (CRC Press, Boca Raton, 2002).
  - [25] "Improved Flow Measurement Accuracy Using Cross-flow Ultrasonic Flow Measurement Technology", West-

- inghouse WCAP-16163-P Rev. 0, 2004.
- [26] W. T. Parry *et al.*, *ASME International Steam Tables for Industrial Use* (ASME Press, New York, 2000).
- [27] The International Association for the Properties of Water and Steam, “Revised Release on the IAPWS Industrial Formulation 1997 for the Thermodynamic Properties of Water and Steam”, 2007, available at <http://www.iapws.org/release.htm> (accessed August 1, 2008).
- [28] “Calibration for Beaver Valley Unit 2 LEFM CheckPlus System”, Caldon Inc. ML129, 2000.
- [29] M. Takamoto and A. Andersson, “What is the volume of one liter?”, IAEA Technical Meeting on Increasing Power Output and Performance of Nuclear Power Plants by Improved Instrumentation and Control Systems, Prague, Czech Republic, 2007.
- [30] V. R. Foster Jr., *Flow Control: The Magazine of Fluid Handling Systems*, Vol. VII, No. 8 (2001).
- [31] L. C. Lynnworth, *Ultrasonic Measurements For Process Control: Theory, Techniques, Applications* (Academic Press, San Diego, 1989).
- [32] “General Electric BWR Thermal Analysis Basis (GETAB): Data, Correlation and Design Application”, General Electric Co. NEDO-10958-A, 1977.
- [33] “Caldon Experience in Nuclear Feedwater Flow Measurements”, Caldon Inc. ML162 Rev. 1, 2002.
- [34] H. Estrada, “An Assessment of the Integrity and Accuracy of Feedwater Flow and Temperature Measurements”, Caldon Inc. TP11 Rev. 2, 1996.
- [35] “Implications of Power Uprates on Safety Margins of Nuclear Power Plants”, IAEA-TECDOC-1418, 2004.
- [36] US Code of Federal Regulations, Title 10, Part 50, Appendix K (2000).
- [37] *Hokkaido Electric Power, Tomari Nuclear Power Plant (Units 1, 2) License Application*, 1986 (in Japanese).
- [38] V. R. Foster Jr., *Flow Control: The Magazine of Fluid Handling Systems*, Vol. VII, No.6, 16 (2001).
- [39] “Improving Thermal Power Accuracy and Plant Safety While Increasing Operating Power Level Using the LEFM System”, Caldon Inc. ER-80P, Rev. 0, 1998 (Caldon Inc. Proprietary).
- [40] H. Estrada, “Identifying and Bounding the Uncertainties in LEFM Flow Measurements”, Caldon Inc. TP-13, 1996.
- [41] US Nuclear Regulatory Commission, “NRC Staff Position on Use of the Westinghouse Crossflow Ultrasonic Flow Meter for Power Uprate or Power Recovery”, Regulatory Issues Summaries 2007-24 (2007).
- [42] D. W. Spitzer, *Flow Measurement* (The Instrumentation, Systems, and Automation Society, Research Triangle Park, 2001).
- [43] “Nuclear Feedwater Flow Measurement Application Guide”, EPRI TR-112118, 1999.
- [44] N. Furuichi, *AIST Bulletin of Metrology*, Vol. II, No. 3, 569 (2005) (in Japanese).
- [45] N. Furuichi *et al.*, “A Facility with High Reynolds Number for Calibration of a Feedwater Flowmeter”, ICONE15-10209, 2007.
- [46] C. E. Sanders and I. C. Gauld, “Isotopic Analysis of High-Burnup PWR Spent Fuel Samples From the Takahama-3 Reactor”, ORNL/TM-2001/259, 2003.
- [47] I. C. Gauld, “Strategies for Application of Isotopic Uncertainties in Burnup Credit”, NUREG/CR-6811, ORNL/TM-2001/257, 2003.
- [48] “User’s Manual for ROCS”, Combustion Engineering Inc. CE-CES-4-Rev. 3-P.
- [49] E. K. Lee *et al.*, *Ann. Nucl. Energy* **26**, 983 (1999).
- [50] K. Suyama *et al.*, *J. Nucl. Sci. Tech.* **39**, 82 (2002).
- [51] K. Suyama, H. Mochizuki, and T. Kiyosumu, *Nucl. Tech.* **138**, 97 (2002).
- [52] Y. Nakahara *et al.*, *Nucl. Tech.* **137**, 111 (2002).
- [53] R. J. Guenther *et al.*, Pacific Northwest National Laboratory Report No. PNL-5109-104, 1991.
- [54] D. E. Burk, M.S. thesis, Texas A&M University, 2005.
- [55] “Standard Test Method for Atom Percent Fission in Uranium and Plutonium Fuel (Neodymium-148 Method)”, American Society for Testing And Materials, E321, 1996.
- [56] “Nuclear Fuel Data”, Energy Information Administration, Form RW-859, 2002, available at [http://www.eia.doe.gov/cneaf/nuclear/spent\\_fuel/ussnftab3.h](http://www.eia.doe.gov/cneaf/nuclear/spent_fuel/ussnftab3.h) (accessed August 1, 2008).
- [57] O. W. Hermann *et al.*, “Validation of the SCALE System for PWR Spent Fuel Isotopic Composition Analysis”, ORNL/TM-12667, 1995.
- [58] O. W. Hermann and M. D. DeHart, “Validation of SCALE(SAS2H) Isotopic Predictions for BWR Spent Fuel”, ORNL/TM-13315, 1998.
- [59] M. D. DeHart and O. W. Hermann, “An Extension of SCALE(SAS2H) Isotopic Predictions for PWR Spent Fuel”, ORNL/TM-13317, 1996.
- [60] “Benchmark of SCALE (SASH2) Isotopic Predictions of Depletion Analysis for San Onofre PWR MOX Fuel”, ORNL/TM-1999/326, 1999.
- [61] Y. Nakahara, K. Suyama, and T. Suzuki, Translation of “Technical Development on Burn-up Credit for Spent LWR Fuel”, JAERI-Tech 2000-071, 2000 [ORNL/TR-2001/01, 2001].
- [62] M. D. DeHart, M. C. Brady, and C. V. Parks, “OECD/NEA Burnup Credit Criticality Benchmark Phase I-B Results”, ORNL-6901, 1996.
- [63] Y. Nakahara *et al.*, *Radiochim. Acta* **50**, 141 (1990).
- [64] G. Zacek *et al.*, *Phys. Rev. D* **34**, 2621 (1986).
- [65] Y. Declais *et al.*, *Phys. Lett. B* **338**, 383 (1994).